

Gap solitons in defocusing lithium niobate binary waveguide arrays fabricated by proton implantation and selective light illumination

Y. Tan · F. Chen · P.P. Belićev · M. Stepić · A. Maluckov ·
C.E. Rüter · D. Kip

Received: 10 December 2008 / Revised version: 26 February 2009 / Published online: 3 April 2009
© Springer-Verlag 2009

Abstract Photovoltaic photorefractive binary waveguide arrays are fabricated by proton implantation and selective light illumination on top of an iron-doped near stoichiometric lithium niobate crystal. Linear discrete diffraction and nonlinear formation of gap solitons were investigated by single-channel excitation using Gaussian light beams coupled into either wide or narrow waveguide channels. The results show that, at low power, linear light propagation leads to discrete diffraction, whilst for higher input power the focusing mechanism dominates, finally leading to the formation of gap solitons in the binary waveguide arrays. Our simulation of light propagation based on a nonlinear beam propagation method confirms the experimental findings.

PACS 42.65.Tg · 42.65.Wi · 61.72.Up

Y. Tan · F. Chen (✉)
School of Physics, Shandong University, 250100 Jinan, China
e-mail: drfchen@sdu.edu.cn
Fax: +86-531-88565167

F. Chen
State Key Laboratory of Crystal Materials, Shandong University,
250100 Jinan, China

P.P. Belićev · M. Stepić
Vinča Institute of Nuclear Sciences, P.O. Box 522,
11001 Belgrade, Serbia

A. Maluckov
Faculty of Sciences and Mathematics, University of Niš,
P.O. Box 224, 18001 Niš, Serbia

C.E. Rüter · D. Kip
Institute of Energy Research and Physical Technologies, Clausthal
University of Technology, 38678 Clausthal-Zellerfeld, Germany

1 Introduction

Wave propagation in periodic media is characterized by a dispersion relation showing both pass bands and stop bands [1]. Within a linear theory, only a wave whose frequency lies outside the stop band may propagate through the system. It is shown that an intense (nonlinear) wave can change the refractive index of the periodic structure in a way to shift itself (i.e., the propagation constant) out of the stop band [2]. Such nonlinear structures reside within the bandgap as a defect and are widely known as gap solitons. In one-dimensional (1D) lattices, gap solitons arise either from the top of even bands in the self-focusing case (positive sign of the nonlinearity) or from the bottom of odd bands in the self-defocusing case (negative sign of the nonlinearity). In optics, the most prominent examples of periodic media are photonic structures [3]. Nonlinear waveguide arrays (WAs) represent one possible realization of such media possessing a periodic refractive index potential. In general, a WA consists of regularly spaced (straight or curved) channel waveguides that are weakly coupled due to evanescent fields. Permanent 1D nonlinear WAs have been fabricated in various materials [4–6], to mention only a few.

Motivated by research of diatomic lattices (i.e., 1D chains made of two atom species with different masses) [7], Sukhorukov and Kivshar have suggested an engineered “binary” array which consists of alternating narrow and wide waveguides [8]. Recently, gap solitons in 1D binary WAs have been observed in a 5 mm-long AlGaAs sample [9]. It is shown that Floquet–Bloch (FB) modes, which represent a natural basis in linear periodic systems, originating from the first band, are localized on the wide channels, whereas FB modes that originate from the second band are mainly localized on narrow channels. Surface effects in binary WAs are studied theoretically in [10].

In this work, we explore, for the first time to the best of our knowledge, linear and nonlinear light propagation in permanent 1D lithium niobate (LiNbO_3) binary WAs exhibiting a saturable self-defocusing nonlinearity [6]. The paper is organized as follows. We explain the corresponding fabrication procedure in the next section. After this, the bandgap structure of the binary array is presented and discrete diffraction is investigated. Section 4 is devoted to nonlinear light propagation, while Sect. 5 concludes the paper.

2 Fabrication of defocusing binary waveguide arrays

The x -cut near stoichiometric LiNbO_3 (SLN) sample used in this work is doped with 0.03 wt% Fe (Fe:SLN), and cut to pieces with dimensions of $2(x) \times 5(z) \times 9.8(y)$ mm³ (the y -axis points along the c -direction of the crystal). One optically polished facet (with a size of 5×10 mm²) of the wafer is implanted by protons at an energy of 500 keV and a dose of 2×10^{16} ions/cm², forming a planar waveguide structure, by using an implanter at the Semiconductor Institute of the Chinese Academy of Sciences. Afterwards, to improve the waveguiding properties, the sample is annealed at 400°C for 30 min in air to remove the color centers induced by the implantation. Finally, input and output facets (with sizes of 2×5 mm²) are polished to allow for coupling light into and out of the sample. The guiding properties (dark mode spectra) of the planar waveguide are characterized by the m -line method (with a linearly polarized He–Ne laser, at wavelength of 632.8 nm) by using a prism coupler (Meticon Model 2010 with a rutile prism, refractive index resolution of $\pm 2 \times 10^{-4}$). The waveguides extraordinary refractive index (n_e) profile is reconstructed from the measured m -line spectrum using a reflectivity calculation method (RCM) [11], and results are shown in Fig. 1.

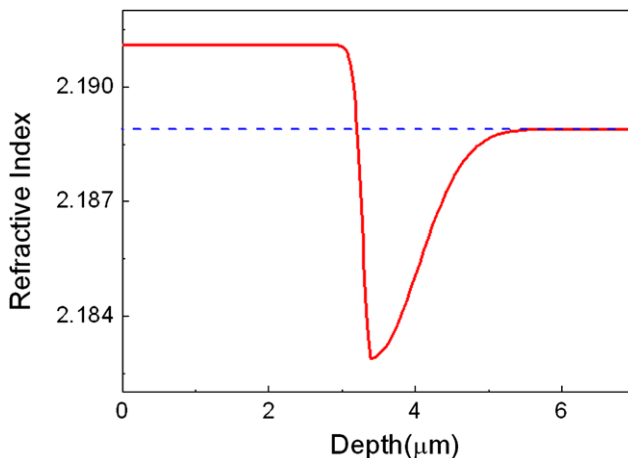


Fig. 1 Refractive index profile n_e of a planar waveguide in Fe:SLN produced by 500 keV proton implantation at a dose of 2×10^{16} ions/cm²

As one can see, the n_e profile consists of a typical “well + barrier”-type distribution, which is in agreement with previous work [12, 13]. The propagation loss of the sample is determined to be ~ 1 dB/cm at 632.8 nm, by measuring scattered light intensity on top of the waveguiding layer versus propagation length.

Figure 2 shows a schematic plot of the WA formation process. A photo mask containing a series of binary stripes is used for selective illumination of the sample surface (i.e., on top of the planar waveguide). The widths of the opaque stripes on the mask are $d_1 = 2 \mu\text{m}$ and $d_2 = 4 \mu\text{m}$ for the narrow and wide structures, respectively. The spacing between the neighboring narrow and wide channels, i.e., the width of the transparent stripes, is $d_3 = 3 \mu\text{m}$. With this mask, an expanded light beam from a linearly polarized green laser (at wavelength of 532 nm) illuminates the sample. Since Fe:SLN is a self-defocusing material, light will reduce the refractive index of the unprotected regions of the mask, whilst having negligible effects on the unexposed planar waveguide layer. Thus, the protected regions (covered by non-transparent stripe mask patterns) in the surface layer form channel waveguides: longitudinally confined by the original planar waveguide, and laterally confined by the light-induced patterns. In this way, the binary array consists of narrow (2 μm) and wide (4 μm) parallel waveguides with an adjacent spacing of 3 μm. The full period of this binary WA is $\Lambda = 12 \mu\text{m}$, and the refractive index modulation is ~ 0.0014 at a wavelength of 632.8 nm. This technique has been successfully used for fabricating reconfigurable channel waveguides and beam splitters in Fe doped LiNbO_3 crystals [14, 15].

3 Bandgap structure and discrete diffraction

The theory of light propagation in periodic media possesses a strong mathematical similarity to the theory of electron waves in crystals: light can propagate in form of so-called Floquet–Bloch modes, which are analog to Bloch modes in solid state physics [16]. Probably the most prominent feature of wave propagation in periodic media is the occurrence of a bandgap structure which can be precisely measured by the prism coupling method; see [17] and references

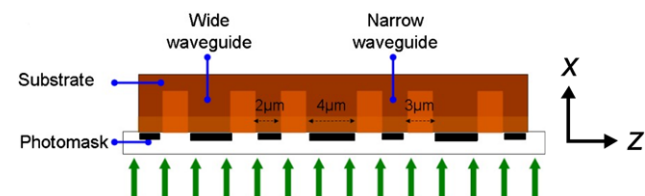


Fig. 2 A schematic plot of the waveguide array formation process. Green light passing an appropriate amplitude mask is used to imprint a transverse modulation on top of the planar waveguide that is formed by ion implantation

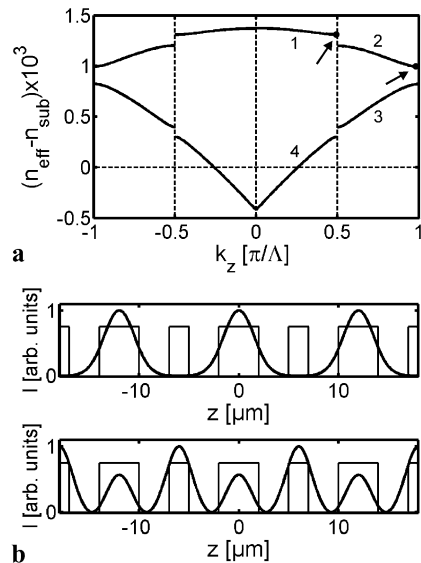


Fig. 3 (a) Bandgap structure of a binary waveguide array (showing bands 1–4) with $d_1 = 2 \mu\text{m}$, $d_2 = 4 \mu\text{m}$, and $d_3 = 3 \mu\text{m}$. The arrows point to the two modes whose amplitude structures are shown in (b), where the upper example corresponds to Bloch modes of band 1 at $k_z = \pi/2\Lambda$ (light guided predominantly in wide channels), whereas the lower example shows a mode in band 2 at $k_z = \pi/\Lambda$ (light guided predominantly in narrow channels)

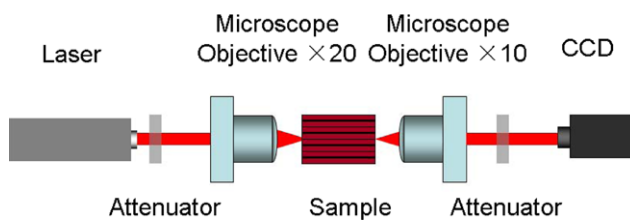


Fig. 4 A schematic plot of the experimental setup for the waveguide excitation and investigation

therein. According to the general theory of light propagation in periodic media [1], we obtain a bandgap structure for TE-polarized light in the $\beta(k_z)$ plane (β being the propagation constant or longitudinal wave vector, and k_z being the transverse wave vector), shown in Fig. 3(a). The two arrows point to the region where modes are excited experimentally by single channel excitation of either broad or narrow channels (please note that, instead of discrete modes corresponding to extended Bloch modes, here we excite a narrow spectrum of modes located around the marked region). The two mode spectra are both located at the bottom of the first two bands. For better illustration, amplitude profiles of the dominating Bloch modes are given in Fig. 3(b), where modes of band 1 are mostly concentrated on the broader channels, while for modes of band 2 amplitude maxima are located on the narrow channels.

Figure 4 shows the schematic plot of the experimental setup. We use a single focused Gaussian beam to excite only one channel. In detail, an extraordinarily polarized

light beam from a He–Ne laser at a wavelength of 632.8 nm passes through an adjustable attenuator, by which the beam power can be controlled. Afterwards, this beam is focused by a $20\times$ microscope objective, and coupled into one channel waveguide (either narrow or wide stripe). After the beam is out-coupled by another $10\times$ microscope objective, a CCD camera is used to measure the exited light intensity distributions on the endfacet.

When the light beam is normally incident into the waveguide, discrete diffraction of light occurs due to the overlap of the modal distributions of adjacent waveguides. We measure the output intensity of the waveguide modes on the endfacet when a single beam is launched either into the narrow (incident power of $0.4 \mu\text{W}$) or wide channels (incident power of $0.1 \mu\text{W}$), as shown in Fig. 5(c) and 5(f), respectively (in-coupled powers inside the WA are lower due to Fresnel reflections and the coupling efficiency which is assumed to be $\sim 50\%$). To ensure linear light propagation, the output images are taken immediately after the beam is launched into the waveguides (i.e., time parameter $t = 0$). For comparison, in Fig. 5(b) and 5(e), we also simulate the corresponding light propagation inside the waveguide arrays using a finite difference beam propagation method (FD-BPM) for the two cases [18]. Here the parameters used in the simulation are exactly related to experimental ones. As one can see, the simulation results are in fairly good agreement with the experimental data. One may note that the narrow waveguide excitation shows stronger diffraction compared to the case of wide channel excitation. From the discrete diffraction spectra, coupling constants $\kappa = \pi/2L_0$ (with L_0 being the coupling length) of $\kappa_{\text{narrow}} = 3.0 \text{ mm}^{-1}$ and $\kappa_{\text{wide}} = 12.8 \text{ mm}^{-1}$ can be obtained. This behavior is expected, as the wider channels allow for stronger guiding of light (i.e., they possess a higher effective refractive index of the respective Bloch modes), which, in turn, results in smaller evanescent fields and thus smaller overlapping with adjacent channels. These findings are in full agreement with the band structure given Fig. 3(a). For example, in the first two bands the curvature $\partial^2\beta/\partial k_z^2$, which is a measure of diffraction, is larger for modes guided in narrow channels (band 2, $\pi/2\Lambda < k_z < \pi/\Lambda$) than for light guided in wide ones (band 1, $0 < k_z < \pi/2\Lambda$).

4 Gap solitons

We investigate nonlinear light propagation and formation of gap solitons by monitoring the time evolution of output light distributions on the endfacet, for excitation of narrow and wide channels, respectively. In both cases, after a certain time, focusing (narrowing) of the light beams is observed, which is due to the negative (defocusing) nonlin-

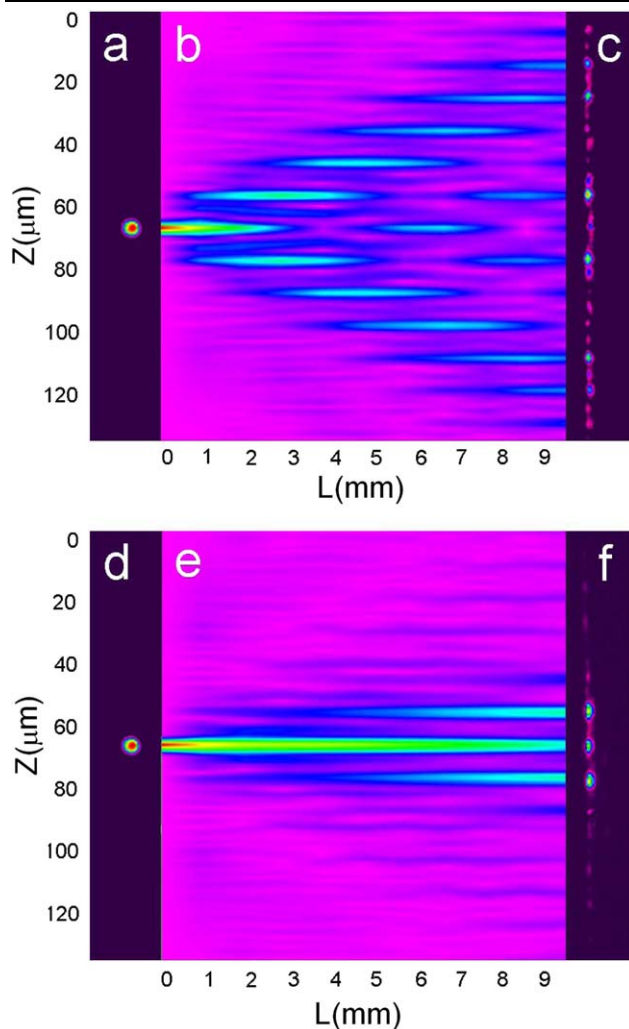


Fig. 5 Experimental and simulation results showing discrete diffraction for linear excitation of the binary WA: (a) and (d) are input Gaussian beams; (b) and (e) show beam propagation inside the binary array; (c) and (f) provide output images of waveguide modal distributions for narrow and wide channel excitations, respectively

earity. We may assume a temporal dependence of refractive index change of the form $\Delta n(t) = \Delta n_0[1 - \exp(-t/\tau)]$, where Δn_0 is the saturated (maximum) index change and τ is the (Maxwell) time constant that is inversely proportional to the in-coupled power. Figures 6(a) and 6(b) depict the optical intensity distribution of the output light for narrow and wide waveguide excitations, respectively. As one can see, in case of a beam launched into the narrow waveguide, after $t = 5$ min, obvious self-trapping can be observed (green line). After $t = 20$ min, a gap soliton is formed (red line), in which the light propagates in a non-diffractive way. However, when a wide channel is excited in Fig. 6(b), a gap soliton is formed already after $t = 4$ min (red line). Taking into account the lower input power used in this case as well as the shorter formation time, a gap soliton is obviously formed for smaller nonlinearity when compared to the case

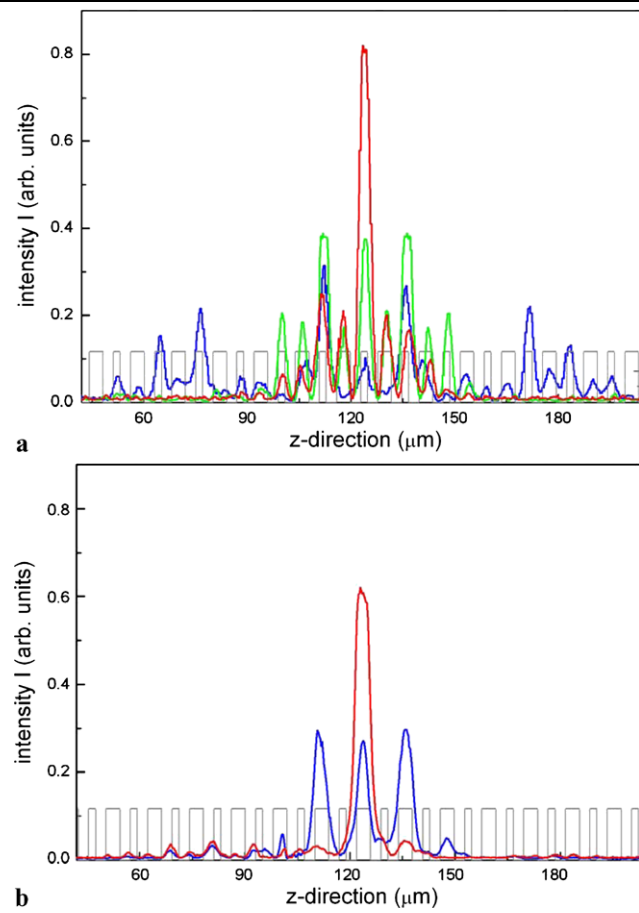


Fig. 6 Optical intensity distribution of the output light for (a) narrow and (b) wide channel excitations. Blue lines denote linear discrete diffraction; green line shows intermediate focusing case; red lines present gap soliton formation. The grey staggered line illustrates the refractive index profile

of narrow-channel excitation. This result is expected, as the light excited in narrow channels shows significantly stronger diffraction, which may be thus compensated by larger nonlinearities. We noticed that, in both cases, the soliton structures do not change for at least 1 hour. Compared with the time of soliton formation, it is reasonable to conclude that the formed structures are stationary stable solitons.

We also use FD-BPM to simulate the nonlinear light propagation in the above two configurations. Figure 7 shows the comparison of simulated light propagation and measured output modal profiles when the gap solitons are formed for narrow (Fig. 7(a–c)) and wide (Fig. 7(d–f)) waveguide channel excitation. Obviously, the numerical simulations confirm the experimental results in a fairly good manner.

5 Conclusion

We report on the fabrication of 1D binary channel waveguide arrays in Fe:SLN crystals by using proton implantation com-

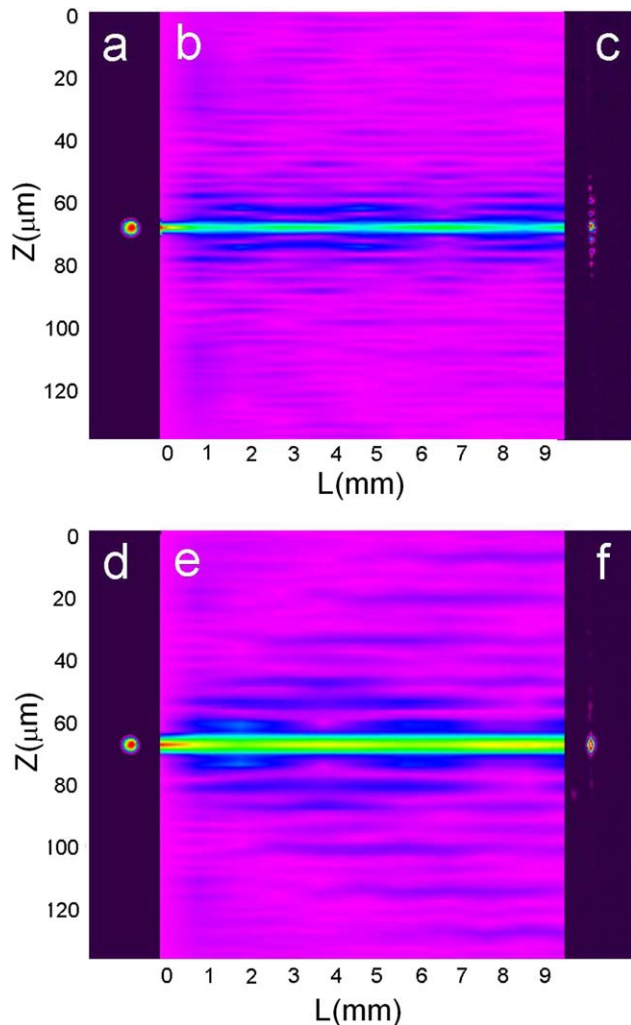


Fig. 7 A comparison of simulated light evolvement and measured output modal profiles when a gap soliton is formed: (a) and (d) show input light beam profiles; (b) and (e) provide beam propagation inside the binary array; (c) and (f) give output images of waveguide modal distributions for narrow and wide channel excitations, respectively

bined with selective light illumination. The linear and nonlinear light propagation in such a photovoltaic binary array

are investigated. At relatively low power of less than 0.4 and 0.1 μW , bright gap solitons are formed when single narrow or wide waveguides are excited, respectively. The numerical calculations confirm our experimental results and verify stable propagation of gap solitons in the array.

Acknowledgements This work is supported by the National Natural Science Foundation of China (NSFC, Grant No. 10505013) and Ministry of Science of Republic Serbia (Project No. 141034) and DFG (grant Ki 482/10-1). F.C. acknowledges financial support of SRF for ROCS, SEM, China.

References

1. P. Yeh, A. Yariv, C.S. Hong, J. Opt. Soc. Am. **67**, 423 (1977)
2. H.G. Winful, J.H. Marburger, E. Garmire, Appl. Phys. Lett. **35**, 379 (1979)
3. J.D. Joannopoulos, S.G. Johnson, J.N. Winn, R.D. Meade, *Photonic Crystals: Molding the Flow of Light*, 2nd edn. (Princeton University Press, Princeton, 2008)
4. H.S. Eisenberg, Y. Silberberg, R. Morandotti, A.R. Boyd, J.S. Aitchison, Phys. Rev. Lett. **81**, 3383 (1998)
5. R. Iwanow, R. Schiek, G.I. Stegeman, T. Pertsch, F. Lederer, Y. Min, W. Sohler, Phys. Rev. Lett. **93**, 113902 (2004)
6. F. Chen, M. Stepić, C.E. Rüter, D. Runde, D. Kip, V. Shandarov, O. Manela, M. Segev, Opt. Express **13**, 4314 (2005)
7. P.C. Dash, K. Patnaik, Phys. Rev. A **23**, 959 (1981)
8. A.A. Sukhorukov, Yu.S. Kivshar, Opt. Lett. **27**, 2112 (2002)
9. R. Morandotti, D. Mandelik, Y. Silberberg, J.S. Aitchison, M. Sorel, D.N. Christodoulides, A.A. Sukhorukov, Yu.S. Kivshar, Opt. Lett. **29**, 2890 (2004)
10. I.L. Garanovich, A.A. Sukhorukov, Yu.S. Kivshar, M. Molina, Opt. Express **14**, 4780 (2006)
11. P.J. Chandler, F.L. Lama, Opt. Acta **33**, 127 (1986)
12. F. Chen, X.L. Wang, K.M. Wang, Opt. Mater. **29**, 1523 (2007)
13. P.D. Townsend, P.J. Chandler, L. Zhang, *Optical Effects of Ion Implantation* (Cambridge University Press, Cambridge, 1994)
14. Y. Tan, F. Chen, M. Stepić, V.M. Shandarov, D. Kip, Opt. Express **16**, 10465 (2008)
15. Y. Tan, F. Chen, X.L. Wang, L. Wang, V. Shandarov, D. Kip, J. Phys. D **41**, 102001 (2008)
16. Z. Zhang, S. Satpathy, Phys. Rev. Lett. **65**, 2650 (1990)
17. C.E. Rüter, D. Kip, Phys. Rev. A **77**, 013818 (2008)
18. Rsoft Design Group, Computer software BEAMPROP version 8.0, <http://www.rsoftdesign.com>